Scilight

Energy Safety Science and Technology
https://www.sciltp.com/journals/esst

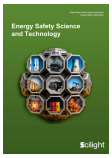

Article

Experimental Study on Suppression of Thermal Runaway Propagation of Lithium-Ion Battery with Parallel Connection by Compressed Air Foams

Ping Ping [1,2,3], Can Yang [4], Depeng Kong [2,3,4,*], Wei Gao [5], Xiantong Ren [4], Xinzeng Gao [4], Xinyu Li [4] and Dongsheng Wang [4]

[1] College of Chemical Engineering, China University of Petroleum (East China), Qingdao 266580, China
[2] State Key Laboratory of Chemical Safety, China University of Petroleum (East China), Qingdao 266580, China
[3] Shandong Key Laboratory of Advanced Electrochemical Energy Storage Technologies, China University of Petroleum (East China), Qingdao 266580, China
[4] College of Mechanical and Electronic Engineering, China University of Petroleum (East China), Qingdao 266580, China
[5] State Key Laboratory of Fine Chemicals, Department of Chemical Machinery and Safety Engineering, Dalian University of Technology, Dalian 116024, China
* Correspondence: kongdepeng@upc.edu.cn

How To Cite: Ping, P.; Yang, C.; Kong, D.; et al. Experimental Study on Suppression of Thermal Runaway Propagation of Lithium-Ion Battery with Parallel Connection by Compressed Air Foams. *Energy Safety Science and Technology* **2026**, *1*(1), 3.

Received: 24 April 2026
Revised: 7 June 2026
Accepted: 12 June 2026
Published: 29 June 2026

Abstract: Lithium-ion batteries (LIBs) have garnered significant attention due to safety concerns associated with thermal runaway propagation (TRP), which may lead to catastrophic fires and explosions. Consequently, preventing and suppressing TRP in LIBs has emerged as an urgent problem demanding immediate solutions. This study systematically evaluates the inhibitory effect of compressed air foams (CAF) on the TRP of LIBs configured in parallel connections. It compares the cooling capabilities of CAF under different gas-liquid ratios and explores the impact of varying application durations and intermittent application strategies on TRP suppression. The results reveal that CAF with a gas-liquid ratio of 6 can effectively suppress the exothermic reactions of the battery. Increasing the application duration significantly enhances the cooling effect of CAF; specifically, an application duration of 180 s effectively suppresses TRP, with an average cooling power increase of 22% compared to a 60 s application. Intermittent application further boosts cooling performance and efficiency, achieving a maximum average cooling power of −123.36 W at a duty cycle (DC) of 0.25, representing a 71% increase compared to continuous application. The combined strategy-first applying intermittent mode (DC = 0.75) to suppress battery thermal reactions, followed by intermittent mode (DC = 0.25) for sustained cooling-maximizes cooling efficiency.

Keywords: lithium-ion battery; parallel connection; compressed-air foams; different gas-liquid ratios; intermittent application

1. Introduction

Lithium-ion batteries (LIBs) are widely used in transportation and energy storage systems due to their advantages of high operating voltage, high specific energy, and long cycle life [1–3]. In recent years, with continuous improvements in manufacturing technologies, the energy density of LIBs has been steadily increasing [4], raising significant concerns about their safety. Thermal abuse [5–7], electrical abuse [8–10], and mechanical abuse [11–13] can potentially lead to thermal runaway in batteries [14]. Once thermal runaway occurs, the battery releases a substantial amount of heat and generates flammable and toxic gases [15,16]. If not promptly controlled,

Copyright: © 2026 by the authors. This is an open access article under the terms and conditions of the Creative Commons Attribution (CC BY) license (https://creativecommons.org/licenses/by/4.0/).
Publisher's Note: Scilight stays neutral with regard to jurisdictional claims in published maps and institutional affiliations.

thermal runaway can propagate, resulting in fire or explosion accidents [17,18]. To ensure the safety of LIBs in practical applications and mitigate environmental pollution caused by such accidents, preventing and suppressing thermal runaway and its propagation in LIBs is an urgent issue that needs to be addressed.

Thermal management technologies, including air cooling [19,20], liquid cooling [21,22], and phase change materials [23–25], have been extensively studied to enhance the safety of LIBs. Despite these efforts, fire and explosion incidents caused by LIBs continue to be reported. Consequently, research has been conducted to investigate the efficacy of various extinguishing agents in mitigating such events. Table 1 summarizes the effectiveness of multiple extinguishing agents in inhibiting thermal runaway propagation (TRP) in battery modules.

Among solid extinguishing agents, dry powder is the most widely employed due to its cost-effectiveness and non-conductive properties, demonstrating efficacy in suppressing LIB fires under appropriate conditions. However, its inherent limitations—particularly inadequate cooling capacity—restrict its ability to mitigate battery TRP. To address this deficiency, Li et al. [26] successfully enhanced TRP suppression by incorporating ammonium aluminum sulfate dodecahydrate (AASD) into the dry powder formulation. Gaseous extinguishing agents, such as CF_3CHFCF_3 (HFC-227ea) [27], $C_6F_{12}O$ (Novec1230) [28,29], and liquid nitrogen [30–32], can rapidly extinguish open flames, leave no residual contamination, and achieve explosion suppression when applied in confined spaces. However, their cooling capacity is limited. HFC-227ea shows almost no inhibitory effect on TRP, while Novec1230 can delay TRP propagation and significantly reduce CO generation. Liquid nitrogen demonstrates the ability to delay TRP in semi-confined environments and performs exceptionally well in confined spaces, where continuous release can completely prevent TRP. Liquid fire suppressants, which typically possess high specific heat capacities and strong cooling capabilities, include water [33], water mist [34–37] and foam extinguishing agents [38–40]. Pure water exhibits high cooling efficiency but requires large volumes and can be detrimental to battery integrity [41]. Water mist, characterized by extremely small droplet sizes and large specific surface areas, rapidly absorbs heat and vaporizes, effectively suppressing TRP when applied continuously. However, it requires longer durations to extinguish large-scale battery fires [30] and faces significant challenges in terms of operational and maintenance costs in practical application [40].

Table 1. Inhibitory effects of various fire extinguishing agents on battery TRP.

Agent	Battery Type	Electrical Connection	Voltage, Capacity and Total Energy	Description
Water	a battery pack composed of hundreds of 38 Ah NCM cells [33]	3P6S 3P5S	22.2 or 18.5 V 114 Ah 2.53 or 2.11 kWh (a battery module)	Large quantities of water can effectively extinguish fires in electric vehicles, but their ability to suppress the propagation of thermal runaway within the internal batteries is relatively poor.
Water mist	six 2.6Ah 18,650 NCM batteries [34]	5P	3.7 V 15.6 Ah 57.72 Wh	Parallel connections can accelerate the propagation of thermal runaway in batteries, leading to critical temperatures below 100 °C. Water primarily relies on sensible heat to cool the batteries, thereby reducing the cooling efficiency of fine water mist.
CAF	a battery pack composed of 1320 2.2 Ah NCM batteries [39]	60P22S	79.2 V 132 Ah 10.45 kWh	A full-scale fire test on an electric vehicle was conducted using compressed air foam, with a foam usage rate of 0.743 m^3/kWh. The fire was extinguished without reignition, but the temperature could not be reduced below 50% °C.
$C_6F_{12}O$	twelve 243 Ah LFP batteries [29]	12S	38. 4V 243 Ah 9.33 kWh	$C_6F_{12}O$ can suppress the temperature of the thermal runaway battery below 300 °C, effectively inhibiting the propagation of thermal runaway.
	twelve 67Ah NCM batteries [28]	3P4S	14.4 V 201 Ah 2.89 kWh	$C_6F_{12}O$, due to its low momentum, struggles to reach the surface of the battery, resulting in poor cooling effects. Increasing its flow rate or using it in conjunction with fine water mist can enhance the cooling performance.
Water mist	five 2.6 Ah 18,650 NCM batteries [35]	--	3.7 V 2.6 Ah 48.1 Wh	A water usage of 1.95×10^{-4} kg Wh^{-1} is sufficient to prevent thermal runaway propagation, with a cooling rate exceeding 100 K s^{-1}, and the surface temperature can be reduced to 373.15 K within a few seconds.

Table 1. *Cont.*

Agent	Battery Type	Electrical Connection	Voltage, Capacity and Total Energy	Description
	three 4 Ah 21,700 NCM batteries [37]	--	3.7 V 4 Ah 44.4 Wh	Water mist exhibits better fire extinguishing performance at a cycle of 2 s with a duty cycle of 0.5, and it provides better cooling effects at a cycle of 20 s with a duty cycle of 0.25. The combined use of these two intermittent modes yields even better results.
	three 2 Ah 18,650 LFP batteries [36]	--	3.2 V 2 Ah 19.2 Wh	A 30-s application of fine water mist is sufficient to suppress the propagation of thermal runaway.
Liquid nitrogen	two 3.5 Ah 18,650 NCM batteries [31]	--	3.7 V 3.5 Ah 25.9 Wh	In confined spaces, 0.18 L of liquid nitrogen is sufficient to suppress the propagation of thermal runaway, with an average cooling rate of 4.06 °C/s during the release period for the thermal runaway battery.
	two 50 Ah LFP batteries [30]	--	3.2 V 50 Ah 320 Wh	In a confined environment, liquid nitrogen can prevent the propagation of thermal runaway; however, in a semi-confined environment, liquid nitrogen can only delay the propagation of thermal runaway.
	fifteen 60 Ah LFP batteries [32]	--	3.2 V 60 Ah 2.88 kWh	Releasing liquid nitrogen from the top of the module can effectively suppress the propagation of thermal runaway, while releasing it from the left side or back cannot inhibit TR propagation.
Composite dry powder	two 3.5 Ah 18,650 NCM batteries [26]		3.7 V 3.5 Ah 25.9 Wh	Adding 50% AASD to the dry powder can inhibit the propagation of thermal runaway, while adding 35% AASD results in only the second battery venting.
$C_6F_{12}O$ water mist	four 2.6 Ah 18,650 NCM batteries [42]	--	3.7 V 2.6 Ah 38.48 Wh	Novec1230 can effectively reduce the formation of CO, while water mist can effectively suppress the propagation of thermal runaway. The combined use of both may yield even better results.
	four 150 Ah NCM batteries [43]	--	3.7 V 150 Ah 2.22 kWh	$C_6F_{12}O$ delayed the propagation of thermal runaway by 427 s, reducing the battery surface temperature to 267 °C; fine water mist can suppress TR propagation, keeping the battery surface temperature below 100 °C.
CF_3CHFCF_3 $C_6F_{12}O$ water mist	two 117 Ah NCM batteries [27]	--	3.7 V 117 Ah 865.8 Wh	HFC-227ea has little effect on the propagation of thermal runaway in confined spaces, while $C_6F_{12}O$ can delay its propagation, and water mist can suppress the spread of thermal runaway.

Note: For module configurations without electrical interconnection, the tabulated voltage and capacity values correspond exclusively to those of individual cells.

Foam extinguishing agents, as a type of liquid extinguishing agent, offer several advantages, including excellent fire suppression performance, strong burn resistance, good fluidity, and ease of storage and transportation. Compressed air foam (CAF), created through the thorough mixture of water, foam concentrate, and air, exhibits high foam momentum and low electrical conductivity. These attributes render CAF highly effective in extinguishing fires involving storage tank [44,45], oil-immersed transformers [46,47], and combustible liquid fuel [48,49]. When applied to LIB fires, CAF rapidly covers the battery surface without causing external short circuits or damage. Additionally, the foam's viscosity allows it to adhere to battery surfaces for extended durations, continuously releasing liquid to provide long-lasting cooling, thereby inhibiting TR and its propagation. Indeed, research on the application of CAF to LIB fires has already been conducted. Andersson et al. [38] conducted experiments using 20 Ah lithium iron phosphate (LFP) batteries and found that low-expansion CAF (with a lower gas-liquid ratio) exhibited superior wetting and cooling effects on the LFP battery fire. Cui et al. [39] performed full-scale fire tests on electric vehicles using CAF, with a foam application rate of 0.743 m^3/kWh. While the fire was successfully extinguished without re-ignition, the temperature could not be reduced below 50 °C. Li et al. [40]

conducted fire suppression tests on 280 Ah LFP cells using compressed nitrogen foam and found that a release pressure of 0.4–0.6 MPa provided the most effective continuous cooling. These studies provide preliminary guidance for CAF in suppressing battery fires. CAF demonstrates rapid fire extinguishment and reignition prevention capabilities. Notably, the gas-liquid mixing ratio is a critical factor influencing the physicochemical properties of CAF, which directly affects its cooling performance on batteries. However, existing research in this area remains limited. Furthermore, prior investigations have focused exclusively on either single-cell TR suppression or full-scale electric vehicle fire containment, while studies specifically addressing LIB TRP inhibition are notably absent.

In addition to the cooling effectiveness of extinguishing agents, the electrical configuration of batteries significantly influences the propagation process of battery TR [50–54]. In practical applications, batteries are electrically connected to form modules, rather than solely through physical contact. Studies have shown that parallel-connected battery configurations exhibit faster TRP rates and pose higher risks compared to series-connected configurations [52,53]. In parallel circuits, a battery undergoing TR may experience internal short circuits, leading to an external short circuit across the entire module. In this scenario, the TR battery acts as a load within the circuit, while the remaining functional batteries continuously supply electrical energy to it. This energy is converted into Joule heating, which not only increases the peak temperature during TR but also accelerates TRP [51,54]. Table 1 summarizes the electrical connection configurations of battery modules, highlighting the limited research on suppressing TRP in electrically connected batteries, which presents a more formidable challenge.

The release strategy of extinguishing agents also significantly impacts their effectiveness in suppressing TRP. For single-agent applications, intermittent application is currently the most prevalent strategy [37,55,56]. An appropriate duty cycle (DC) and application interval can enhance the cooling performance of extinguishing agents. Zhang et al. [37] demonstrated that water mist exhibits superior fire suppression performance at a 2-s cycle with a 0.5 DC, while a 20-s cycle with a 0.25 DC provides better cooling effects. The synergistic use of these two intermittent modes yields optimal results. CAF, known for its rapid coverage of battery surfaces, could potentially benefit from an intermittent release strategy. Timely replenishment of foam after depletion may further improve its cooling efficiency.

Current research exhibits gaps in investigating the cooling performance of CAF at varying gas-liquid ratios (GLRs) and its effectiveness in suppressing TRP for parallel-connected batteries. Furthermore, there is a pressing need to develop more efficient CAF application strategies. Therefore, this study aims to investigate the inhibitory effects of CAF on TRP in parallel-connected battery configurations. By systematically altering the GLR, the influence of this parameter on the cooling capacity of CAF will be systematically examined. Furthermore, the study will adjust the duration of continuous CAF application to evaluate its impact on TRP suppression. Finally, a comparative analysis of the cooling effectiveness of different DCs under intermittent application strategies will be conducted, providing new insights into the mitigation of TRP.

2. Experimental

2.1. Experimental Apparatus

Figure 1 presents a schematic diagram of the experimental setup. The setup includes a combustion chamber, a gas exhaust system, a CAF system (CAFS), and an integrated data acquisition system. The foam is vertically released through a pipe installed 20 cm above the battery. Additionally, the CAFS is primarily composed of a foam generator, a foam container, a pump, an air compressor, and two flowmeters and allows for adjustment of the GLR. The performance parameters corresponding to different GLRs of the foam are shown in Table 2. The GLR was set between 6 and 10 to balance foam expansion, wettability, stability, and adhesion. A lower GLR may result in insufficient foam expansion and poor surface coverage, whereas an excessively high GLR reduces foam wettability and effective contact with the battery surface. Therefore, GLR values of 6, 8, and 10 were selected to evaluate the cooling performance of CAF under representative foam expansion conditions. The foam solution used in this study is a mixture of 3% aqueous film-forming foam (AFFF) and water, with a liquid flow rate of 0.7 L/min.

Table 2. Performance parameters corresponding to different GLRs of the foam.

Type of Foam Concentrate	GLRs	Gas Flow (L/min)	Liquid Flow (L/min)	Foaming Multiple
3% AFFF	6:1	4.2	0.7	9.2
	8:1	5.6		9.9
	10:1	7.0		10.4

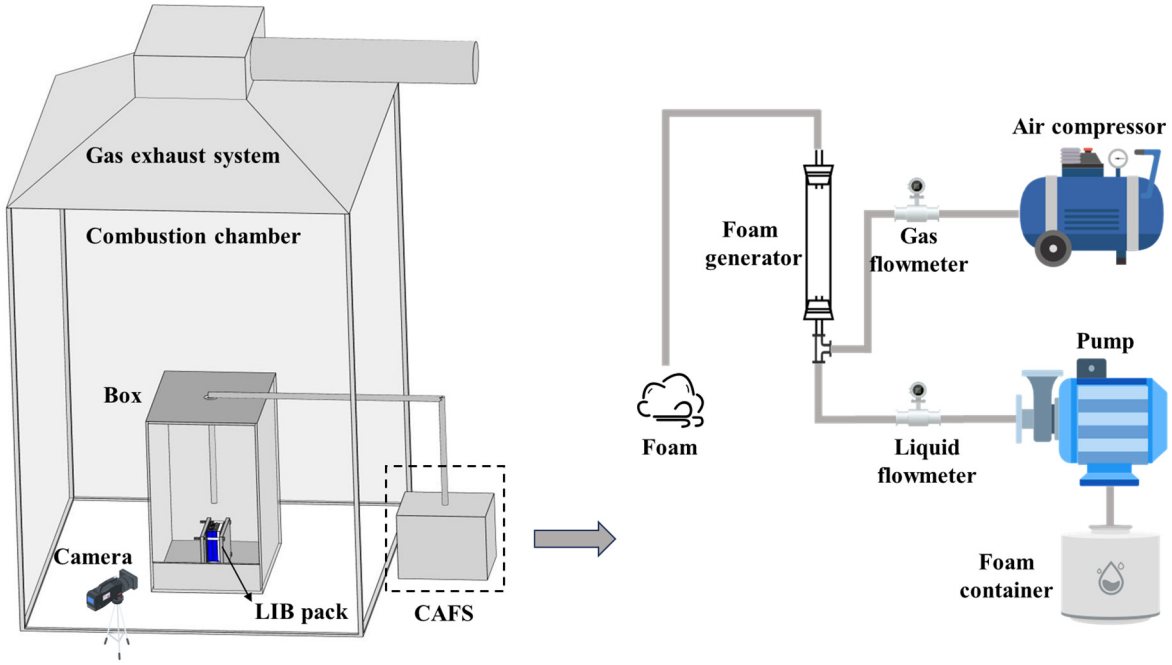

Figure 1. Schematic diagram of the experimental setup.

2.2. Battery Samples

This study investigates 30Ah prismatic $LiFePO_4$ batteries. Each sample was fresh and charged to full state of charge (SOC) at a rate of 1/3 C before the experiment. The dimensions of the battery are 101 mm in length, 22 mm in width, and 145 mm in height, with a mass of 620 g. Figure 2 illustrates the arrangement of the battery pack and thermocouples. To initiate TR in battery #1, a 600W heating plate is applied to the side of the battery. Insulating plates are placed on both sides and subjected to a predetermined pressure using steel plates to ensure complete contact. This arrangement simulates the characteristics of a battery pack with inadequate heat dissipation. As shown in Figure 2b, five thermocouples are set up for each battery to record temperature changes during the experiment. The average surface temperature of the battery can be calculated using Equation (1).

$$T_{ave} = \frac{T_f + T_s + T_u + T_b + T_d}{5} \quad (1)$$

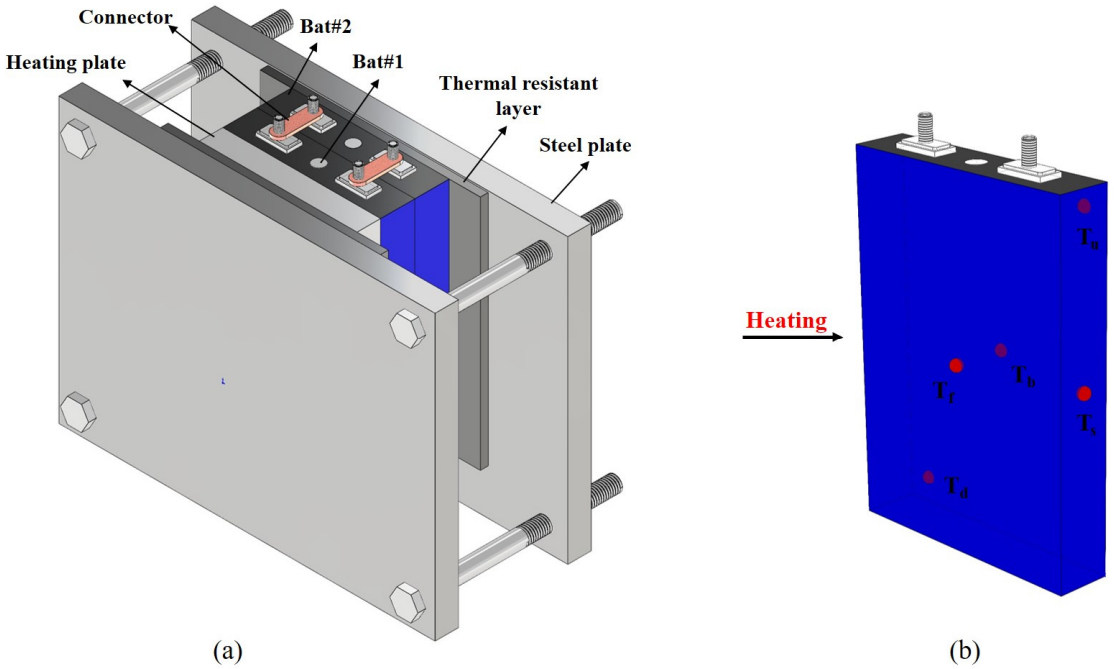

Figure 2. Schematic diagram of the (**a**) LIBs and (**b**) TCs arrangement.

2.3. Experimental Design

Table 3 presents a comprehensive summary of the experimental conditions applied in this study. Experiments 1–4 are designed to compare the inhibitory effects and cooling performance of CAF with different GLRs on battery TR. Experiments 5–7 assess the effects of different CAF application durations on TRP, with Experiment 5 serving as a baseline to explore TRP in a parallel battery module without any intervention. Additionally, experiments 8–10 examine the impact of different DCs on TRP suppression. Intermittent application involves multiple cycles, each consisting of an application period and an interval. The DC is defined as the ratio of application period to the total cycle duration. Across all experiments, the application cycle is standardized to 60 s, and Figure 3 provides a detailed description of these application modes. To guarantee experimental repeatability and data reliability, all tests adopted new batteries of identical specifications, which were fully charged under the same conditions prior to testing. Uniform settings were maintained for battery placement, heating power and position, thermocouple arrangement, CAF application height, liquid flow rate and data acquisition system. Each battery was fitted with five thermocouples to monitor temperature distribution, and the average surface temperature was calculated to mitigate local temperature fluctuations. The consistent correlations among temperature, voltage, venting and heat accumulation further verified the validity of experimental data.

Table 3. Key parameters of the experimental conditions.

Test	Electrical Connection	GLR	Apply Duration (s)	Doses (L)	Duty Cycle	Apply Cycle (s)
1	single battery	--	--	--	--	--
2		6:1	60	0.7	--	--
3		8:1	60	0.7	--	--
4		10:1	60	0.7	--	--
5	parallel connection	--	--	--	--	--
6		6:1	60	0.7	--	--
7		6:1	180	2.1	--	--
8		6:1	180	2.1	0.25	60
9		6:1	180	2.1	0.5	60
10		6:1	180	2.1	0.75	60

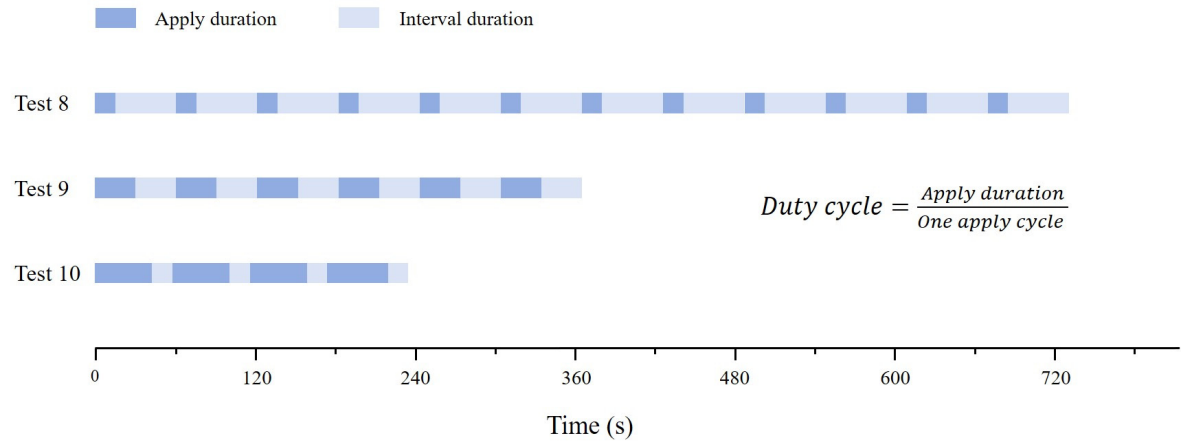

Figure 3. Detailed explanation of application modes.

3. Results and Discussion

3.1. Suppression Effect of CAF on TR of Single Battery

3.1.1. TR Behavior of Single Battery

Figure 4 illustrates the temperature changes of a single battery during its free-burning process. The TR process of the battery can be broadly divided into four stages: the heat accumulation phase, the combustion phase, the intense smoke production phase, and the natural cooling phase. As the heating plate continuously inputs heat to the battery, a series of exothermic reactions occur within the battery, continuously generating gas and increasing internal pressure. Around 520 s, the safety valve ruptures, and the internal gas of the battery is expelled. At this point, the temperature on the backside of the battery reaches 94.67 °C. After manual ignition, the battery undergoes violent combustion, with flames reaching the top of the explosion-proof box. Subsequently, the flames gradually

stabilize and continue to burn for approximately 100 s. At 710 s, the battery experiences a complete internal short circuit, leading to a sudden and drastic increase in gas production, which extinguishes the flames as they are forcefully expelled. At this juncture, the battery enters the intense gas production phase, with a sharp increase in temperature, reaching a peak of 425.99 °C. Around 900 s, the smoke gradually dissipates, and the battery enters the natural cooling phase. CAF will be challengingly released during the intense gas production phase of the battery to explore its inhibitory effect on the battery's exothermic reactions in extreme cases.

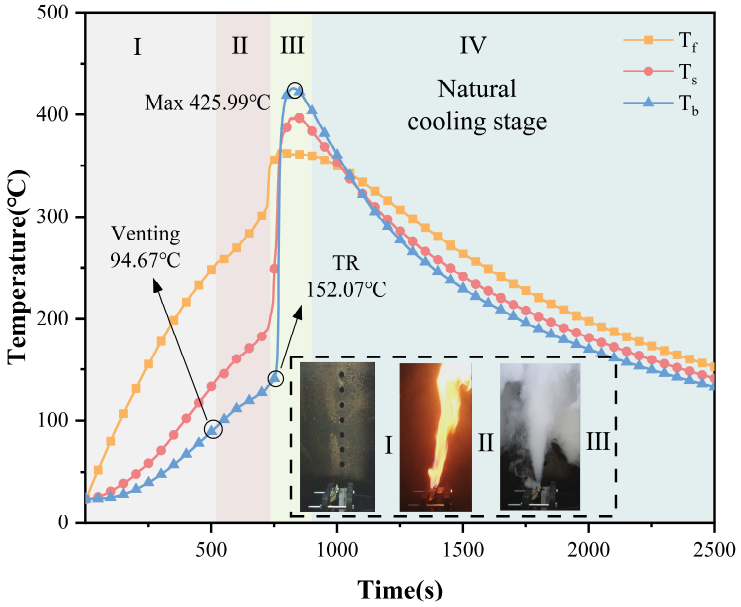

Figure 4. Surface temperature changes of single battery.

3.1.2. Suppression Effect of CAF in Different GLRs

Figure 5a shows the temperature changes of individual batteries under different GLRs of CAF applied for 60 s. After the application of CAF, there is a significant reduction in the highest surface temperatures of the batteries, and the onset time of TR is delayed by an average of approximately 35 s. This indicates that the release of CAF has a certain inhibitory effect on the internal thermal reactions of the batteries. When CAF with GLR of 6 and 10 is applied, the highest surface temperatures of the batteries are similar, at 320.35 °C and 318.46 °C, respectively. Compared to Test 1 without CAF application, these temperatures are reduced by 63.7 °C and 65.59 °C, respectively. However, the battery with GLR of 8 has the highest surface temperature at 328.80 °C, with a reduction of only 55.25 °C. The lower the highest surface temperature of the battery, the better the inhibitory effect of the extinguishing agent on the exothermic reaction of the battery.

Figure 5b shows the duration of high temperatures and mass loss of the batteries after applying CAF for 60 s under different GLRs. Referring to CCCF/XFJJ-01 [57], the duration of high temperatures above 150 °C is a key indicator in assessing the efficacy of cooling-type extinguishing devices; the longer this duration, the stronger the thermal hazard and the higher the potential risk of TRP. Additionally, the mass loss of the battery can serve as an indicator of the severity of TR, helping to evaluate the effectiveness of the extinguishing agent in mitigating the internal reactions of the battery. The battery without CAF release has a high-temperature duration of 1853 s, while in the three test groups with CAF release, the high-temperature duration is 1385 s for GLR of 8, 1364 s for GLR of 10, and the shortest high-temperature duration is 1283 s for GLR of 6. The corresponding mass losses are 126.8 g, 122.5 g, 122.6 g, and 119.1 g, respectively. These findings illustrate the cooling and inhibitory effects of CAF on the exothermic reactions of the batteries, with the most significant effect observed at a GLR of 6. When the GLR is excessively high, the expanded volume of the foam increases significantly. This not only slows down the drainage rate but also reduces the effective contact area with the battery surface. As a result, the amount of water flowing through the battery decreases, leading to a reduction in cooling efficiency. Conversely, when the GLR is too low, the foam's expansion ratio becomes insufficient, preventing effective coverage and adhesion to the battery. This causes rapid water loss, thereby diminishing the long-lasting cooling performance. Among the tested GLRs, GLR = 6 provides the optimal suppression effect because it achieves a favorable balance between wettability, foam expansion, adhesion, and drainage. A higher GLR produces lighter foam with reduced wettability and a smaller effective contact area with the battery surface, making it more susceptible to disturbance by the intense gas flow generated during thermal runaway. In contrast, an excessively low GLR may weaken foam

stability and reduce the duration of surface coverage. Therefore, CAF with GLR = 6 can maintain effective adhesion and coverage while continuously releasing liquid to form a cooling film, resulting in the most effective suppression of battery thermal reactions. Finally, CAF with GLR of 6 will be applied in subsequent tests to evaluate its inhibitory effect on TRP.

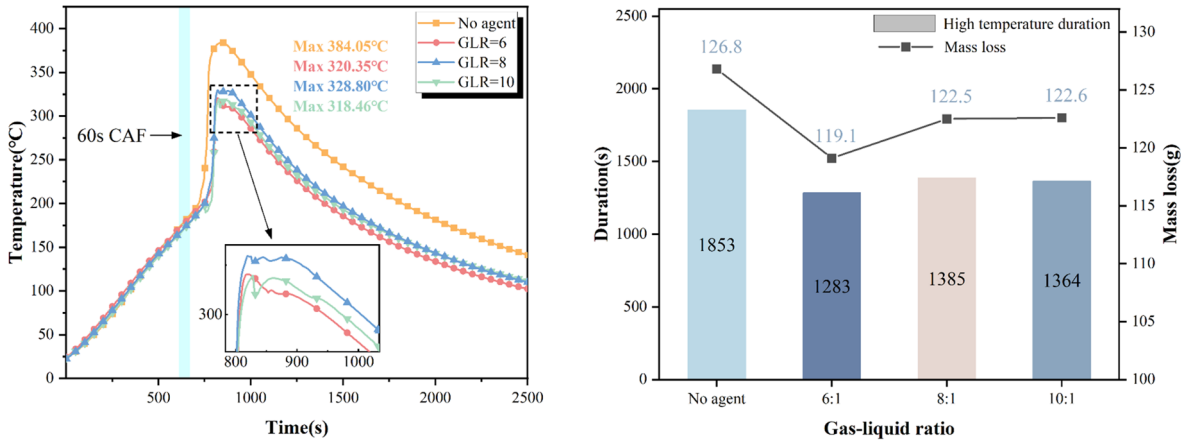

Figure 5. (**a**) Average surface temperature and (**b**) high temperature duration and mass loss under different GLR of CAF applied.

3.2. Suppression Effect of CAF on TRP

3.2.1. TRP Behavior of Parallel Connected Module

Figure 6a depicts the temperature changes on the backside of the battery module. Due to the layered structure within the batteries, the temperature changes on the backside can effectively reflect the extent of internal thermal reactions. Based on the temperature variations on the backside of the batteries, the TRP of the battery module can be roughly divided into four stages: the self-heating stage of battery #1, the electrical energy conversion stage, the self-heating stage of battery #2, and the natural cooling stage. Stage I: Intense exothermic reactions occur within battery #1, producing a large amount of smoke and heat, causing the temperature to rapidly rise to 431.31 °C before briefly dropping to 404.83 °C. Stage II: Battery #1, which has already undergone TR, experiences a complete internal short circuit, acting as an external load for battery #2. Subsequently, battery #2 continuously transfers its own electrical energy to battery #1, and the significant amount of Joule heat generated causes the temperatures of both batteries to rise, with battery #1 reaching a peak temperature of 524.91 °C. Stage III: Under the heat transfer from battery #1 and its own internal thermal reactions, battery #2 violently ejects dense smoke and undergoes TR. At this point, the TRP of the module is complete. Stage IV: The smoke gradually dissipates, and the batteries cool naturally in the environment. Due to the parallel connection causing a secondary temperature rise in battery #1, its thermal hazard is greater than that of a battery without electrical connection, and the temperature rise time of battery #1 is prolonged, which means a longer application time of the extinguishing agent is required to effectively suppress the battery's thermal reactions. Figure 6b shows the surface temperature changes of the battery module during free-burning. Battery #1 vents at 622 s, and battery #2 completes venting at 926 s. Due to the influence of electrical energy transmission through the parallel connection, the backside of battery #1 and the front side of battery #2 both experience a secondary temperature rise, with peak temperatures of 524.91 °C and 560.84 °C, respectively. Because battery #2 consumes some of its own electrical energy, the peak temperature on its backside is only 361.64 °C, significantly lower than the peak temperature on the backside of battery #1.

Figure 7 illustrates the module voltage changes during the free-burning phase of the battery module. Starting at 785 s, continuous internal reactions within battery #1 cause the module voltage to begin a gradual decline. At 805 s, the voltage drops to 2.52 V, at which point battery #1 undergoes TR. Following this, the voltage rebounds and fluctuates, always remaining below the module's initial voltage. This is because, post-TR, battery #1, having experienced a complete internal short circuit, acts as a load across the terminals of battery #2. Consequently, battery #2 discharges energy into battery #1, leading to a reduction in its SOC and a consequent lower voltage. The voltage fluctuations are attributed to the excessive surface temperature following TR, which melts the insulating plastic casing surrounding the batteries. With the outer packaging removed, the batteries make direct contact, establishing additional electrical connections beyond parallel linkages, thereby affecting the module voltage. Ultimately, at 992 s, battery #2 also undergoes TR, causing the module voltage to drop to 0 V. Since the

fluctuation of module voltage occurs later than the venting time of the battery, detecting voltage changes for accident early warning is not a good choice; however, it is effective in assessing the degree of battery damage.

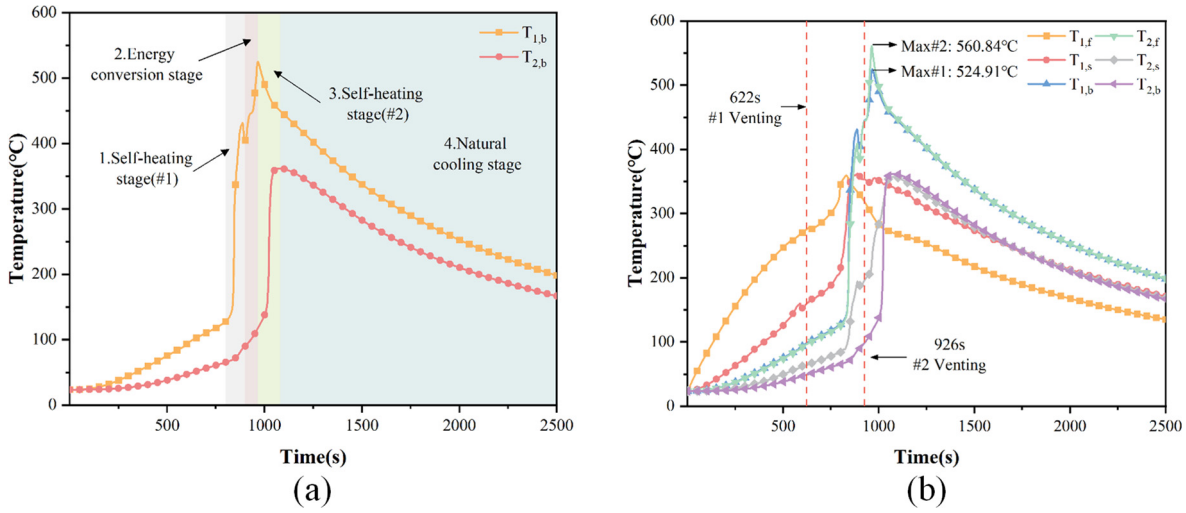

Figure 6. Temperature changes of (**a**) back and (**b**) surface of batteries.

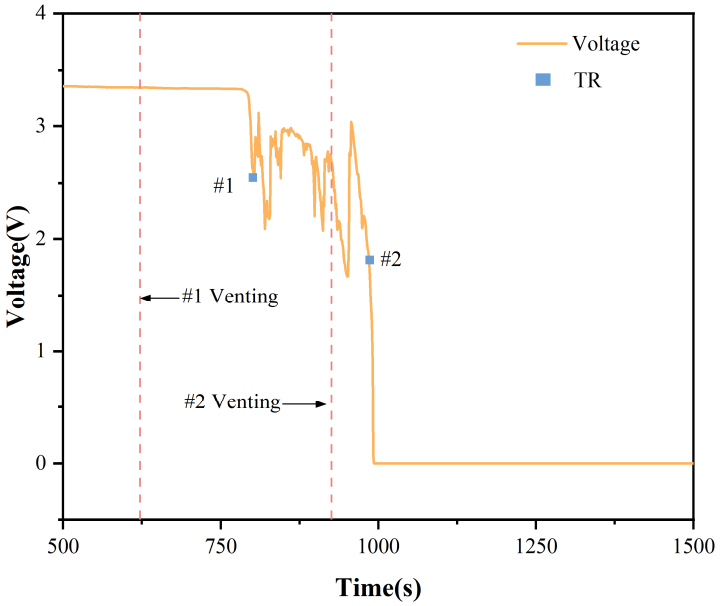

Figure 7. Voltage changes of battery module with parallel connection.

3.2.2. Suppression Effect of CAF under Different Application Durations

Figure 8 illustrates the inhibitory effects of CAF on TRP with varying application durations. CAF is applied after the intense gas emission from battery #1, increasing the challenge of suppressing TRP. At 900 s, a 60 s CAF release concludes and blankets the battery surface. However, its limited cooling capacity does not prevent battery #1 from heating battery #2. Battery #2 gradually heats up and vents gas at 1276 s. Two seconds later, the gas is ignited by the red-hot nuts on the electrodes. Eventually, the flames gradually extinguish around 1500 s. When CAF is applied for 180 s, the foam completely envelops the batteries, and the prolonged cooling prevents battery #2 from venting. Correspondingly, Figure 9a shows the surface temperature changes of the batteries during a 180 s CAF release. The peak surface temperatures of batteries #1 and #2 are 358.71 °C and 295.15 °C, respectively, which are 166.20 °C and 265.69 °C lower than those in Test 5. Moreover, battery #2 does not vent, successfully suppressing TRP. The side temperature of battery #1 experiences a decrease from 233.39 °C to 166.53 °C and then an increase during the continuous application of CAF. This is because the front and back sides of the battery are closely packed and cannot directly interact with the extinguishing agent. Therefore, the extinguishing agent first reduces the side temperature, creating a temperature gradient that gradually cools the interior of the battery. In contrast to the significant reduction in the side temperature of battery #1, the side temperature of battery #2 only

decreases from 106.07 °C to 101.17 °C. This is because the release of CAF significantly lowers the surface temperature of battery #1, reducing the heat transferred to battery #2. With a lower surface temperature on battery #2, the smaller temperature difference diminishes the heat exchange with the extinguishing agent, resulting in a mere 4.9 °C temperature reduction.

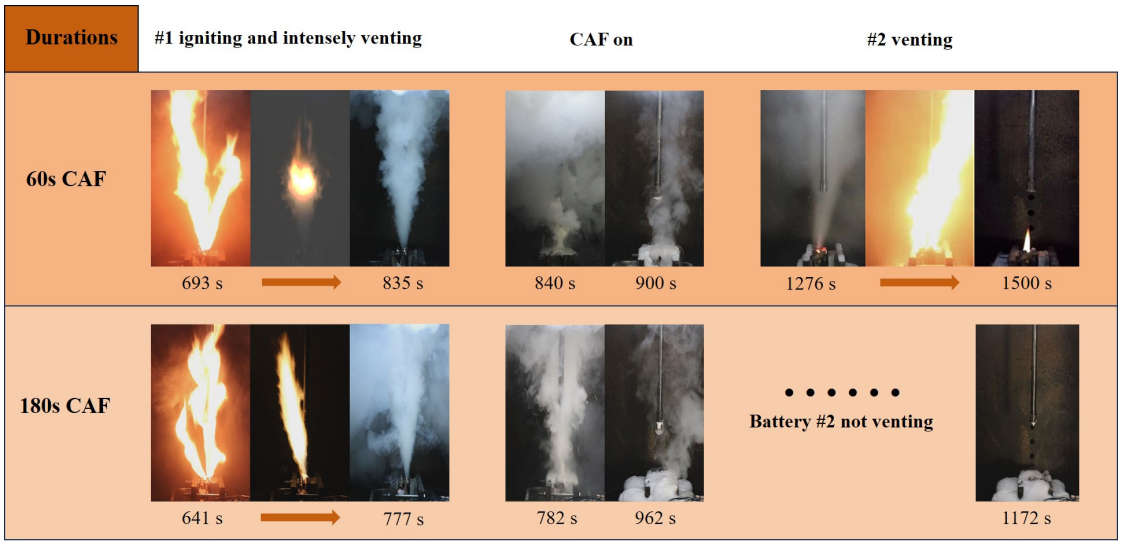

Figure 8. Suppression of TRP by CAF.

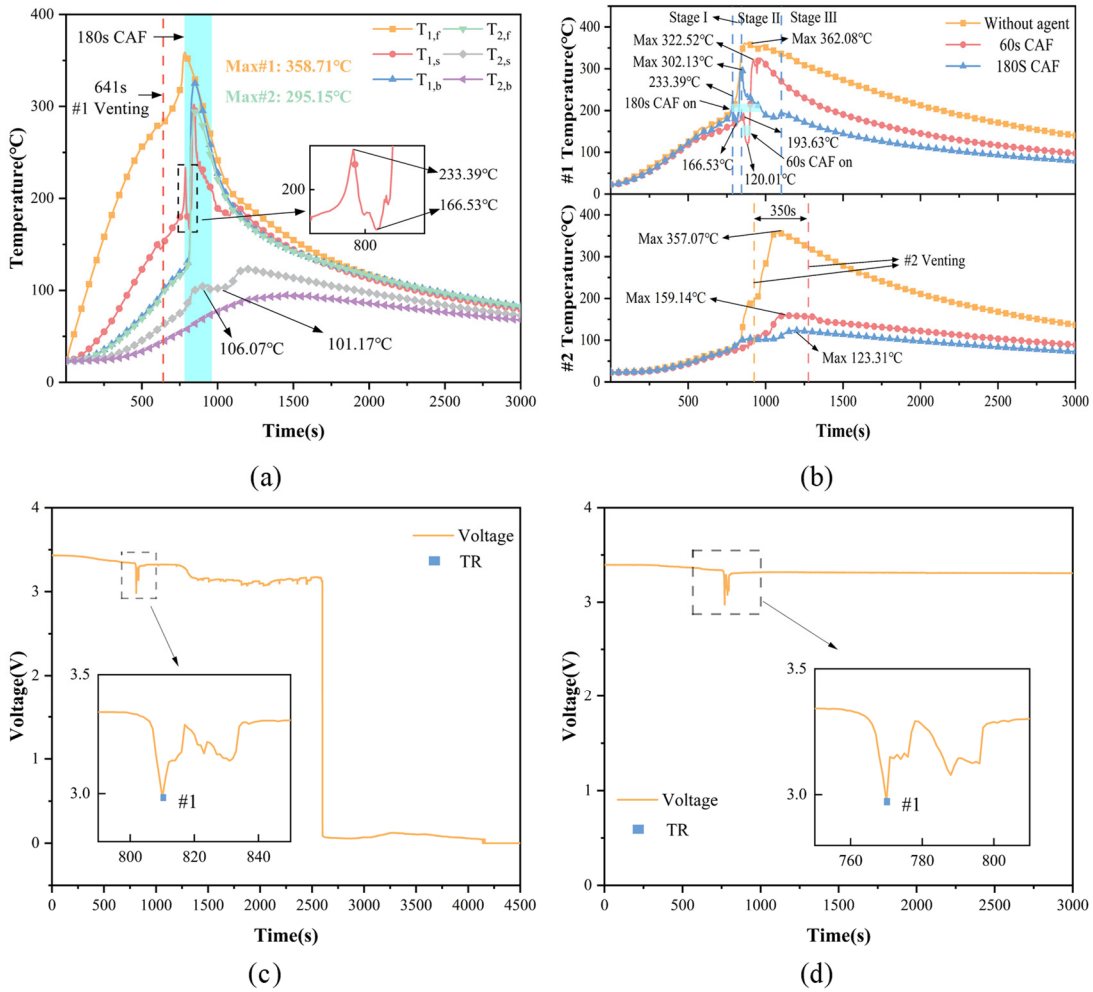

Figure 9. (**a**) Surface temperature changes of batteries under 180 s CAF; (**b**) side temperature of batteries under different application durations of CAF; voltage changes of battery module by application of (**c**) 60 s CAF and (**d**) 180 s CAF.

Since the side of the battery can directly interact with the extinguishing agent, its temperature changes can more intuitively reflect the cooling effect on the battery after the application of the extinguishing agent. Figure 9b shows the impact of CAF application duration on the side temperature of the batteries. For the scenarios where CAF is applied for 60 s and 180 s, the peak temperatures of battery #1 after TR are 322.52 °C and 302.13 °C, respectively. Compared to the scenario without the application of an extinguishing agent, the peak TR temperatures are reduced by 39.56 °C and 59.95 °C, respectively. When CAF is applied for 60 s, the venting time of battery #2 is delayed by 350 s, and when CAF is applied for 180 s, battery #2 does not vent at all. This indicates that the longer the application time of CAF, the better the inhibitory effect on TRP. The temperature curve of battery #1 shows three stages of temperature decline: the first (Stage I) is the temperature drop caused by the application of CAF, with the side temperature of the battery dropping from 193.63 °C to 120.01 °C and from 233.39 °C to 166.53 °C under two different conditions. The second (Stage II) occurs after the application of CAF ends, due to the continuous drainage by CAF causing a temperature drop. When the heat taken away by the drainage is less than the heat generation of the battery, there will be a temporary temperature rise, followed by the third temperature drop (Stage III), which is the natural cooling phase. For ease of discussion in subsequent sections, let the application time of the extinguishing agent be denoted as t_a, the effective cooling time as t_e, the effective drainage time as t_p, and the long-lasting cooling efficiency as η. They satisfy the following relationship:

$$t_e = t_a + t_p \tag{2}$$

$$\eta = \frac{t_p}{t_a} \tag{3}$$

where t_e is the time from the start of the extinguishing agent application to the point before the secondary temperature rise, and t_p is the time from the end of the extinguishing agent application to the point before the secondary temperature rise. For scenarios where CAF is applied for 60 s and 180 s, the t_e values are 104 s and 295 s, respectively, both of which are greater than t_a. This confirms the sustained cooling capability of CAF, which can continuously reduce the battery temperature through the drainage.

Figure 9c illustrates the voltage changes in the battery module with 60 s CAF application. Similar to the voltage changes without the application of CAF, the voltage gradually decreases as the separator melts, reaching its lowest value of 2.98 V at 810 s, at which point battery #1 undergoes TR. Subsequently, the voltage rebounds, and the value after the rebound is lower than the initial voltage, also due to the energy loss from battery #2. At 1235 s, the voltage slowly decreases again, and after dropping to 3.15 V, it undergoes minor fluctuations for approximately 1200 s. This is because the cooling capacity of the 60 s CAF is insufficient; battery #1 continues to heat battery #2 at a low power state, causing slow internal reactions within battery #2. At 2599 s, the module voltage suddenly drops to 0.1V, and finally, at 4160 s, the voltage drops to 0 V. Interestingly, although the module voltage dropped to 0 V, battery #2 only vented without undergoing TR. This may be because the continuous heating from battery #1 caused most of the separators within battery #2 to melt, but due to the low thermal power, it only resulted in an internal short circuit without an abnormal temperature increase. Figure 9d shows the voltage changes in the battery module with 180 s CAF application. At 770 s, battery #1 undergoes TR, and the module voltage drops to 2.97 V before rebounding, which is also lower than the initial voltage, for the reasons previously described. The voltage then remains around 3.31 V, and after the experiment, it is observed that the plastic casing of battery #2 remains intact, indicating that battery #2 only suffered minor damage and TRP was successfully suppressed. These findings emphasize the importance of the long-lasting cooling capability of the extinguishing agent. Under the 60 s CAF, although the temperature of battery #2 did not surge, it still led to battery failure, increasing economic losses.

The heat accumulation (H_A) and heating power (P_h) of a battery are key parameters for characterizing TR. Where H_A is the energy accumulation that leads to an increase in battery temperature, complying with the principle of energy conservation and P_h represents the rate of energy accumulation. These values can be approximately calculated using Equations (4) and (5) [30,58]:

$$H_A = H_{transfer} + H_{flame} + H_{tr} - H_{loss} - H_{vent} = cm(T_{ave} - T_{amb}) \tag{4}$$

$$P_h = \frac{dH_A}{dt} \tag{5}$$

where $H_{transfer}$ represents the heat transfer from the heating plate or the TR battery. H_{flame} is the heat transfer from the battery flame, which includes both thermal convection and thermal radiation. H_{tr} is the heat generated within the battery due to side reactions and internal short circuits. H_{loss} is the heat loss and H_{vent} is the heat loss due to

venting. c =1 kJ·kg^{-1}·℃$^{-1}$ is the specific heat capacity of the battery. m is the mass of the battery. T_{amb} is the ambient temperature (22 °C).

TRP is primarily caused by the massive heat generation following the TR of battery #1, hence, the heat accumulation of battery #1 is a key parameter in assessing the inhibitory effect of fire suppressants on TRP. The maximum heat accumulation without the application of fire suppressants is the theoretical maximum heat (H_{the}). The maximum heat accumulation with the application of fire suppressants is the actual maximum heat (H_{act}). Furthermore, fire suppressants can not only remove residual heat from the lithium-ion battery module but also inhibit the thermal reactions within the batteries. The heat generated by exothermic reactions that would have occurred but were inhibited by the application of CAF (H_{inb}) can be determined by Equation (6)[37]:

$$H_{inb} = H_{the} - H_{act} \tag{6}$$

To facilitate subsequent comparisons of the cooling effects of various CAF release strategies and to eliminate the impact of natural cooling, the average heating power within 600 s after the heat accumulation reaches its peak is defined as the average cooling power ($P_{c,ave}$). This value can reflect the long-lasting cooling capability of CAF on the battery. Figure 10 illustrates the dynamic changes in heat accumulation (H_A) and heating power (P_h) of the battery under different CAF application durations. For the scenarios with 0 s, 60 s, and 180 s of CAF application, the corresponding maximum heat accumulations for battery #1 are 229.41 kJ, 172.47 kJ, and 161.13 kJ, respectively. Compared to the scenario without CAF application, the maximum heat accumulations have all decreased to varying degrees, with H_{inb} values of 56.94 kJ and 68.28 kJ, respectively. This indicates that the application of CAF suppresses the thermal reactions of the battery, and the inhibitory effect on the battery's thermal reactions is enhanced with the extension of the duration. Correspondingly, the maximum heat accumulations for battery #2 are 219.12 kJ, 80.55 kJ, and 64.07 kJ. In Equation (4), due to the application of CAF, both the heat transfer from battery #1 to battery #2 ($H_{transfer}$) and the intrinsic thermal reactions of battery #2 (H_{tr}) are effectively suppressed, leading to a reduction in the heat accumulation of battery #2. The corresponding $P_{c,ave}$ values for the three scenarios are −47.90 W, −59.17 W, and −71.98 W. Compared to the scenario without CAF application, the application of 60s CAF and 180 s CAF increased $P_{c,ave}$ by 24% and 50%, respectively. This demonstrates that the cooling capacity is enhanced with the increase in CAF application time and reaffirms the long-lasting cooling capability of CAF.

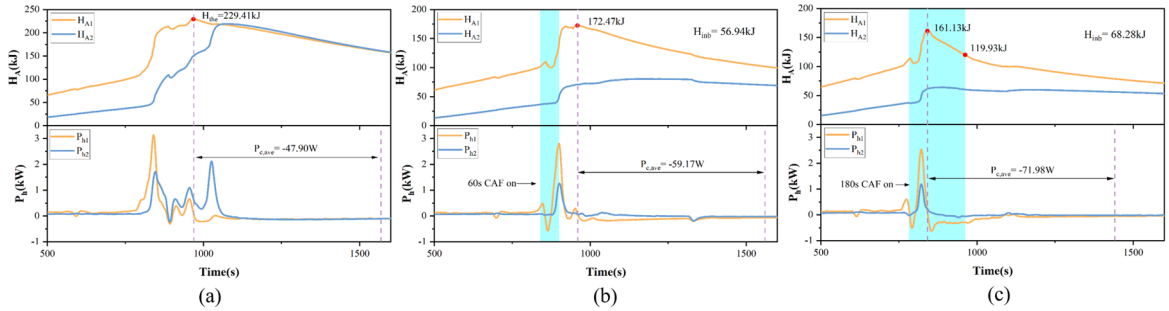

Figure 10. Heat accumulation and heating power of batteries with (**a**) no agent, (**b**) 60 s CAF and (**c**) 180 s CAF.

3.2.3. Suppression Effect of CAF under Intermittent Application

Figure 11 reveals the correlation between different durations of CAF application and its long-lasting cooling efficiency. When t_a increases from 60 s to 180 s, the corresponding η values decrease from 0.73 to 0.64, a reduction of approximately 12%. This indicates that while extending the application time of CAF can enhance cooling capacity, it also leads to a waste of the extinguishing agent. After CAF has covered the surface of the battery, the subsequently applied CAF slides off the surface of the already existing CAF without coming into contact with the battery, thereby reducing cooling efficiency. The cooling effect of CAF has a certain longevity; it needs a certain amount of time to complete the drainage after covering the battery surface, and the 180s constant application apparently overlooks this point. Considering the characteristics of CAF, an intermittent release strategy would be an effective way to improve cooling efficiency. This section will explore the impact of different duty cycles of intermittent application on the cooling effect of CAF.

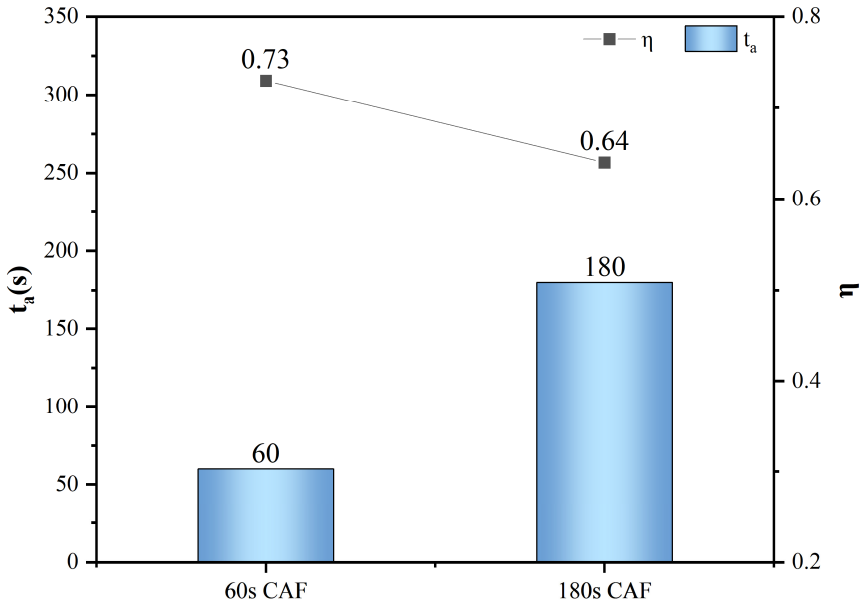

Figure 11. Changes of t_a and η with different durations of CAF.

Table 4 compares the high-temperature duration and characteristic temperature parameters of battery #1. Referring to CCCF/XFJJ-01 [57], attention is given to the temperature 900 s after TR (T_{900}). This temperature can reflect the long-lasting cooling capability of the fire suppressant on the battery. Compared to the scenario without CAF application, the high-temperature duration, T_{max}, and T_{900} of all groups are significantly reduced. As the duty cycle (DC) decreases, the high-temperature duration and T_{900} gradually decrease, while T_{max} gradually increases. The T_{900} for the intermittent application with a DC of 0.25 is only 107.9 °C, which is the lowest. The T_{900} for DC of 0.5 and 0.75 are 141.3 °C and 148.03 °C, respectively. The T_{900} for continuous application is 150.28 °C, slightly higher than the 150 °C specified by CCCF/XFJJ-01. The enhancement of the long-lasting cooling effect of CAF with intermittent application is significant, with the best results at a DC of 0.25. Applying the same dose of CAF, the T_{900} at a DC of 0.25 decreased by 42.38 °C compared to the T_{900} of continuous application, a reduction of up to 28%, and the high-temperature duration was reduced by 176 s.

Table 4. High-temperature duration and characteristic temperature parameters of battery #1.

Application Modes	No agent	CS	DC = 0.25	DC = 0.5	DC = 0.75
T_{max}(°C)	390.24	280.63	313.80	304.93	299.51
T_{900}(°C)	306.47	150.28	107.90	141.30	148.03
Duration(s)	2284	796	620	668	769

Figure 12 illustrates the dynamic changes in H_A and P_h under intermittent application conditions of different duty cycle, and Figure 13 shows the comparison of H_{inb} and $P_{c,ave}$ under different release methods. Intermittent application is more efficient in the utilization of fire suppressants, as it can remove more heat compared to constant application. The absolute value of $P_{c,ave}$ increases as DC decreases. The intermittent spray with DC of 0.25 has the best cooling effect, with a $P_{c,ave}$ of −123.36 W, which is a 71% increase compared to the constant application scenario. The $P_{c,ave}$ values for DC of 0.5 and 0.75 are −107.98 W and −88.95 W, respectively, and both exhibit better cooling effects than constant application. The phenomenon is attributable to the physical distribution of the foam. In contrast to constant application, intermittent application reduces the ineffective loss of foam and extends the duration of effective foam coverage, thereby facilitating more substantial heat exchange. The cooling efficacy is compromised when foam continues to be released after covering the battery or when the battery generates smoke violently. In the former scenario, only a small portion of the subsequently released foam remains on the battery surface, with the majority sliding off the pre-existing foam layer, thus diminishing heat exchange. In the latter case, the foam fails to reach the battery surface altogether. Evidently, intermittent application can more effectively address this issue, with the optimal effect achieved when the DC is set at 0.25. However, constant application is more effective in suppressing the exothermic reactions of the battery than intermittent application. The value of H_{inb} under intermittent application conditions decreases as DC decreases and is less than the H_{inb} value of constant application. This is because the application time of intermittent application does not fully cover the exothermic

reaction phase of the battery, and the liquid released by the already applied CAF has limited inhibitory capacity against exothermic reactions.

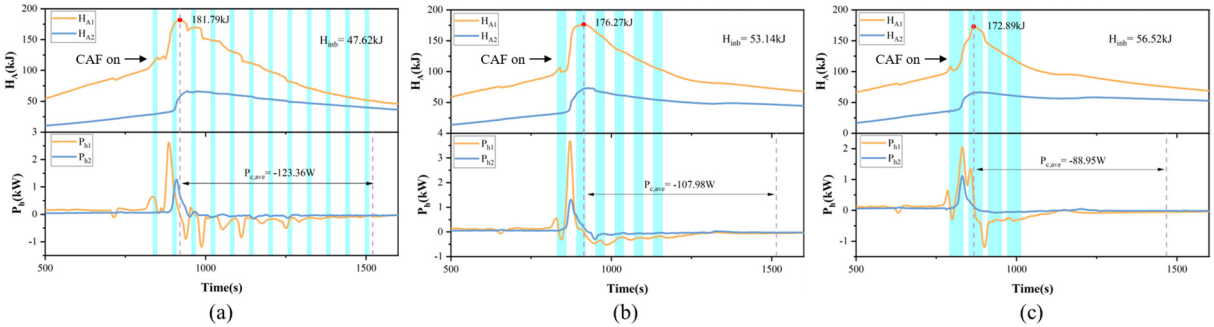

Figure 12. Heat accumulation and heating power of batteries with different DC (**a**) 0.25 (**b**) 0.5 (**c**) 0.75.

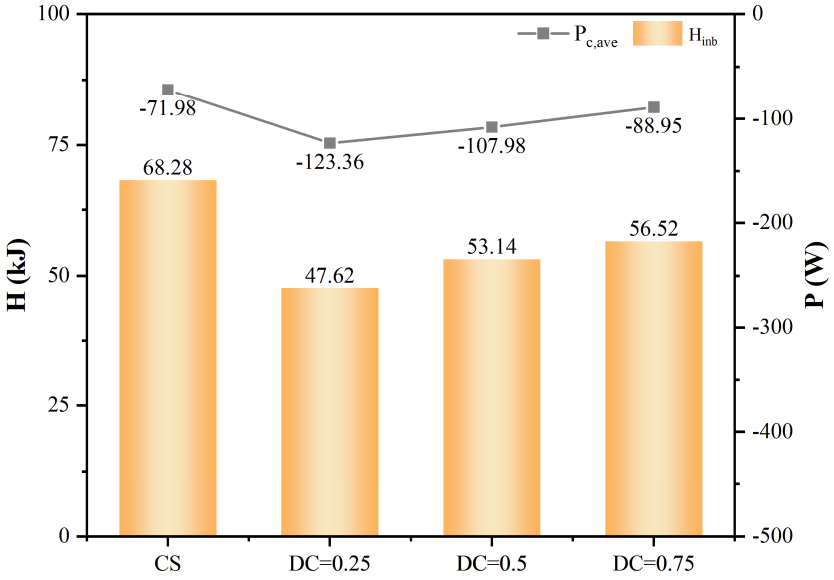

Figure 13. Changes of H_{inb} and $P_{c,ave}$ with different DC.

Figure 14 provides a detailed illustration of the suppression mechanisms of CAF. After covering the battery surface, CAF continuously releases liquid, forming a water film on the battery surface that provides sustained cooling. Additionally, the foam reduces heat radiation and prevents fire reignition. When applied intermittently at the same dosage, CAF reduces ineffective foam loss, extends coverage duration, and enhances the average cooling power. Constant application and intermittent application each have their own advantages. Constant application can most effectively suppress the exothermic reactions of the battery, while intermittent application can enhance the long-lasting cooling effect of CAF. Moreover, the inherent drainage characteristic of CAF gives it longevity in cooling, making it suitable for an intermittent release strategy. When applying CAF in practice, its drainage time should be taken into full consideration, and new CAF should be supplemented in time before the drainage stops. Specifically, intermittent application (DC = 0.75) demonstrates superior suppression of thermal reactions and effectively inhibits TRP, while intermittent application (DC = 0.25) achieves higher extinguishing agent utilization and optimal cooling performance. The combined strategy-first applying intermittent mode (DC = 0.75) to suppress battery thermal reactions, followed by intermittent mode (DC = 0.25) for sustained cooling-maximizes cooling efficiency, suppresses battery TRP, and minimizes accident hazards.

The combined intermittent strategy should be implemented according to the thermal state of the battery module. When abnormal temperature rise, venting, smoke emission, or other early warning signals indicate the onset of thermal runaway, the DC = 0.75 mode can be applied first to provide intensive CAF coverage and suppress strong exothermic reactions. After the intense reaction stage is controlled and the temperature rise rate decreases, the system can switch to DC = 0.25 to maintain long-lasting cooling with higher extinguishing-agent utilization. In this study, the intermittent application cycle was 60 s and the total CAF application duration was 180 s. The proposed strategy therefore provides a staged control concept, while the specific intervention time and switching

duration should be further optimized according to battery module scale, battery chemistry, SOC, detection threshold, and CAF system response time.

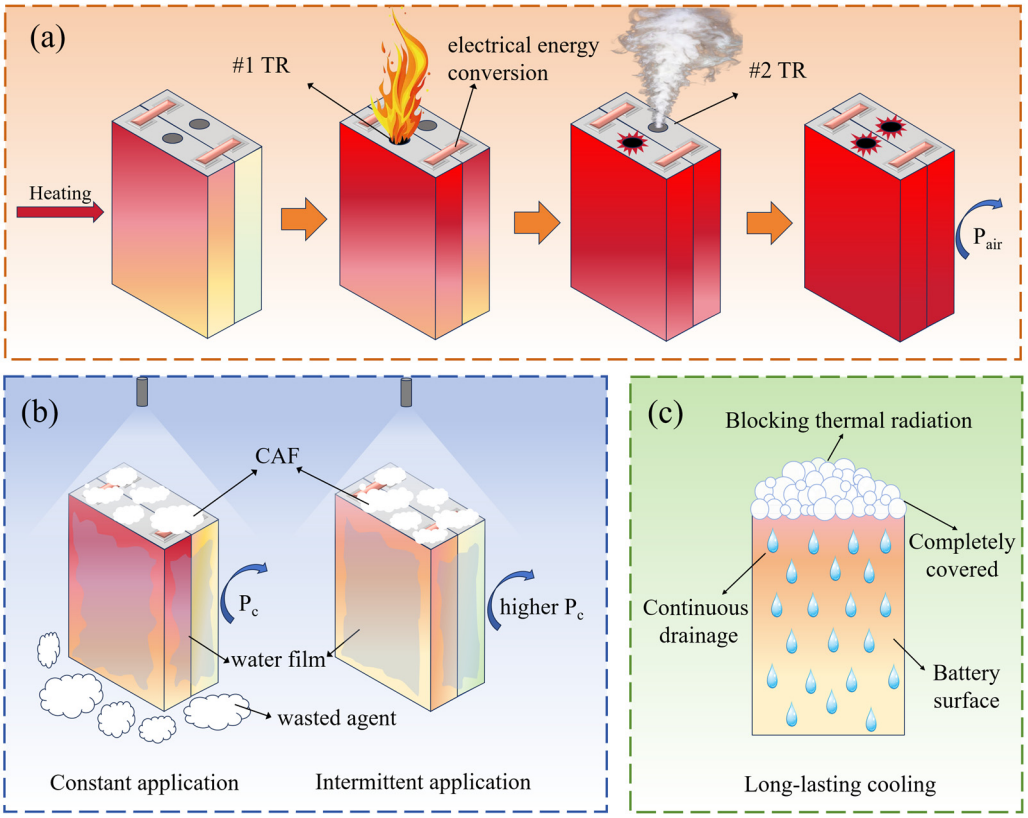

Figure 14. The detailed inhibition mechanism of CAF: (**a**) TR propagation behaviors in the test; (**b**) inhibition mechanism under constant and intermittent application; (**c**) the mechanism of CAF action.

4. Conclusions

This work evaluates the inhibitory effect of CAF on TRP of LIBs. It compares the cooling capacity of CAF under different GLR conditions and investigates the impact of varying application durations and intermittent application strategies on the suppression of TRP. The main conclusions are as follows:

(1) Under the premise of ensuring foam performance, the CAF with a GLR of 6 demonstrates the most effective suppression of TR and provides the best subsequent cooling effect for the battery. The maximum surface temperature of the battery is reduced by 63.7 °C, which can effectively minimize the heat transfer from the TR-affected battery to adjacent batteries.

(2) Parallel connections can exacerbate the thermal hazards of batteries, and increasing the CAF application time enhances its cooling effect. Extending the application time to 180 s maintains battery #2 below the critical temperature, effectively suppressing TRP. Compared to a 60 s CAF application, the average cooling power is increased by 22%. However, the long-lasting cooling efficiency is reduced by 9%, indicating that prolonged application leads to waste of the foam.

(3) Intermittent application can effectively enhance cooling efficiency. The average cooling power increases as the DC decreases, with the maximum average cooling power achieved at a DC of 0.25, reaching −123.36 W. This represents a 71% increase compared to constant application.

(4) Intermittent application (DC = 0.75) demonstrates superior suppression of thermal reactions and effectively inhibits TRP, while intermittent application (DC = 0.25) achieves higher extinguishing agent utilization and optimal cooling performance. The combined strategy-first applying intermittent mode (DC = 0.75) to suppress battery thermal reactions, followed by intermittent mode (DC = 0.25) for sustained cooling-maximizes cooling efficiency, suppresses battery TRP, and minimizes accident hazards.

The present results provide practical guidance for the design of fire suppression protocols in grid-scale battery energy storage systems. For battery modules or packs in which thermal runaway has already initiated, CAF should not only be selected based on its fire-extinguishing capability but also on its ability to provide sustained cooling through foam drainage. The staged intermittent application strategy proposed in this study, namely using a higher

DC to suppress intense thermal reactions followed by a lower DC to maintain long-lasting cooling, may help reduce extinguishing-agent consumption while delaying or preventing thermal runaway propagation in energy storage modules.

Author Contributions

P.P.: investigation, original draft writing, experimental data collection; C.Y.: methodology design, foam performance testing, data analysis; D.K.: conceptualization, supervision, funding acquisition, manuscript review & editing; W.G.: theoretical analysis, literature sorting, validation of experimental mechanism; X.R.: thermal runaway test operation, visualization of experimental curves; X.G.: parallel battery module assembly, raw data curation; X.L.: parameter comparison analysis, table collation; D.W.: resource provision, experiment platform construction, review advice. All authors have read and agreed to the published version of the manuscript.

Funding

This work is financially supported by the National Natural Science Foundation of China (Grant No. U22A20168 and 52174225) and the National Key Research and Development Program (Grant No. 2022YFE0207400). D.K. acknowledges the financial support from Shandong Provincial Natural Science Foundation (No. ZR2023YQ044), and the Shandong Provincial Taishan Scholar Program (No. tsqn202408092).

Conflicts of Interest

The authors declare no conflict of interest.

Use of AI and AI-Assisted Technologies

No AI tools were utilized for this paper.

References

1. Kong, D.; Wang, G.; Ping, P.; et al. A coupled conjugate heat transfer and CFD model for the thermal runaway evolution and jet fire of 18650 lithium-ion battery under thermal abuse. *eTransportation* **2022**, *12*, 100157. https://doi.org/10.1016/j.etran.2022.100157.
2. Tepe, B.; Jablonski, S.; Hesse, H.; et al. Lithium-ion battery utilization in various modes of e-transportation. *eTransportation* **2023**, *18*, 100274. https://doi.org/10.1016/j.etran.2023.100274.
3. Wang, G.; Ping, P.; Kong, D.; et al. Advances and challenges in thermal runaway modeling of lithium-ion batteries. *Innovation* **2024**, *5*, 100624. https://doi.org/10.1016/j.xinn.2024.100624.
4. Feng, X.; Ouyang, M.; Liu, X.; et al. Thermal runaway mechanism of lithium ion battery for electric vehicles: A review. *Energy Storage Mater.* **2018**, *10*, 246–267. https://doi.org/10.1016/j.ensm.2017.05.013.
5. Wang, G.; Ping, P.; Zhang, Y.; et al. Modeling thermal runaway propagation of lithium-ion batteries under impacts of ceiling jet fire. *Process Saf. Environ. Prot.* **2023**, *175*, 524–540. https://doi.org/10.1016/j.psep.2023.05.047.
6. Wang, Q.; Jiang, L.; Yu, Y.; et al. Progress of enhancing the safety of lithium ion battery from the electrolyte aspect. *Nano Energy* **2019**, *55*, 93–114. https://doi.org/10.1016/j.nanoen.2018.10.035.
7. Xu, G.; Huang, L.; Lu, C.; et al. Revealing the multilevel thermal safety of lithium batteries. *Energy Storage Mater.* **2020**, *31*, 72–86. https://doi.org/10.1016/j.ensm.2020.06.004.
8. Mei, W.; Zhang, L.; Sun, J.; et al. Experimental and numerical methods to investigate the overcharge caused lithium plating for lithium ion battery. *Energy Storage Mater.* **2020**, *32*, 91–104. https://doi.org/10.1016/j.ensm.2020.06.021.
9. Ren, D.; Feng, X.; Lu, L.; et al. Overcharge behaviors and failure mechanism of lithium-ion batteries under different test conditions. *Appl. Energy* **2019**, *250*, 323–332. https://doi.org/10.1016/j.apenergy.2019.05.015.
10. Shan, T.; Wang, Z.; Zhu, X.; et al. Explosion behavior investigation and safety assessment of large-format lithium-ion pouch cells. *J. Energy Chem.* **2022**, *72*, 241–257. https://doi.org/10.1016/j.jechem.2022.04.018.
11. Huang, X.; Xue, J.; Xiao, M.; et al. Comprehensive evaluation of safety performance and failure mechanism analysis for lithium sulfur pouch cells. *Energy Storage Mater.* **2020**, *30*, 87–97. https://doi.org/10.1016/j.ensm.2020.04.035.
12. Liu, B.; Jia, Y.; Yuan, C.; et al. Safety issues and mechanisms of lithium-ion battery cell upon mechanical abusive loading: A review. *Energy Storage Mater.* **2020**, *24*, 85–112. https://doi.org/10.1016/j.ensm.2019.06.036.
13. Mallarapu, A.; Kim, J.; Carney, K.; et al. Modeling extreme deformations in lithium ion batteries. *eTransportation* **2020**, *4*, 100065. https://doi.org/10.1016/j.etran.2020.100065.
14. Wei, D.; Zhang, M.; Zhu, L.; et al. Study on Thermal Runaway Behavior of Li-Ion Batteries Using Different Abuse Methods. *Batteries* **2022**, *8*, 201. https://doi.org/10.3390/batteries8110201.

15. Xu, C.; Fan, Z.; Zhang, M.; et al. A comparative study of the venting gas of lithium-ion batteries during thermal runaway triggered by various methods. *Cell Rep. Phys. Sci.* **2023**, *4*, 101705. https://doi.org/10.1016/j.xcrp.2023.101705.
16. Xu, L.; Wang, S.; Li, Y.; et al. Thermal runaway propagation behavior and gas production characteristics of NCM622 battery modules at different state of charge. *Process Saf. Environ. Prot.* **2024**, *185*, 267–276. https://doi.org/10.1016/j.psep.2024.03.011.
17. Said, A.O.; Lee, C.; Stoliarov, S.I.; et al. Comprehensive analysis of dynamics and hazards associated with cascading failure in 18650 lithium ion cell arrays. *Appl. Energy* **2019**, *248*, 415–428. https://doi.org/10.1016/j.apenergy.2019.04.141.
18. Wang, Q.; Ping, P.; Zhao, X.; et al. Thermal runaway caused fire and explosion of lithium ion battery. *J. Power Sources* **2012**, *208*, 210–224. https://doi.org/10.1016/j.jpowsour.2012.02.038.
19. Chen, K.; Chen, Y.; She, Y.; et al. Construction of effective symmetrical air-cooled system for battery thermal management. *Appl. Therm. Eng.* **2020**, *166*, 114679. https://doi.org/10.1016/j.applthermaleng.2019.114679.
20. Li, X.; Zhao, J.; Yuan, J.; et al. Simulation and analysis of air cooling configurations for a lithium-ion battery pack. *J. Energy Storage* **2021**, *35*, 102270. https://doi.org/10.1016/j.est.2021.102270.
21. Li, X.; Zhou, Z.; Zhang, M.; et al. A liquid cooling technology based on fluorocarbons for lithium-ion battery thermal safety. *J. Loss Prev. Process Ind.* **2022**, *78*, 104818. https://doi.org/10.1016/j.jlp.2022.104818.
22. Ping, P.; Du, J.; Dai, X.; et al. A novel dual-purpose thermal runaway propagation mitigation system using a liquid cooling pipe with aperture sealed by films. *J. Energy Storage* **2023**, *71*, 108131. https://doi.org/10.1016/j.est.2023.108131.
23. Dai, X.; Kong, D.; Du, J.; et al. Investigation on effect of phase change material on the thermal runaway of lithium-ion battery and exploration of flame retardancy improvement. *Process Saf. Environ. Prot.* **2022**, *159*, 232–242. https://doi.org/10.1016/j.psep.2021.12.051.
24. Dai, X.; Ping, P.; Kong, D.; et al. Heat transfer enhanced inorganic phase change material compositing carbon nanotubes for battery thermal management and thermal runaway propagation mitigation. *J. Energy Chem.* **2024**, *89*, 226–238. https://doi.org/10.1016/j.jechem.2023.10.001.
25. Ping, P.; Dai, X.; Kong, D.; et al. Experimental study on nano-encapsulated inorganic phase change material for lithium-ion battery thermal management and thermal runaway suppression. *Chem. Eng. J.* **2023**, *463*, 142401. https://doi.org/10.1016/j.cej.2023.142401.
26. Li, X.; Zhang, M.; Zhou, Z.; et al. A novel dry powder extinguishant with high cooling performance for suppressing lithium ion battery fires. Case Stud. *Therm. Eng.* **2023**, *42*, 102756. https://doi.org/10.1016/j.csite.2023.102756.
27. Sun, H.; Zhang, L.; Duan, Q.; et al. Experimental study on suppressing thermal runaway propagation of lithium-ion batteries in confined space by various fire extinguishing agents. *Process Saf. Environ. Prot.* **2022**, *167*, 299–307. https://doi.org/10.1016/j.psep.2022.09.016.
28. Liu, Y.; Liu, J.; Zhao, Z.; et al. The efficiency of dodecafluoro-2-methylpentan-3-one in suppressing NCM 811 lithium-ion battery fire. *Process Saf. Environ. Prot.* **2024**, *186*, 1432–1446. https://doi.org/10.1016/j.psep.2024.04.033.
29. Zhang, L.; Ye, F.; Li, Y.; et al. Experimental Study on the Efficiency of Dodecafluoro-2-Methylpentan-3-One on Suppressing Large-Scale Battery Module Fire. *Fire Technol.* **2022**, *59*, 1247–1267. https://doi.org/10.1007/s10694-022-01322-2.
30. Ping, P.; Gao, X.; Kong, D.; et al. Experimental study on the synergistic strategy of liquid nitrogen and water mist for fire extinguishing and cooling of lithium-ion batteries. *Process Saf. Environ. Prot.* **2024**, *188*, 713–725. https://doi.org/10.1016/j.psep.2024.05.077.
31. Wang, Z.; Wang, K.; Wang, J.; et al. Inhibition effect of liquid nitrogen on thermal runaway propagation of lithium ion batteries in confined space. *J. Loss Prev. Process Ind.* **2022**, *79*, 104853. https://doi.org/10.1016/j.jlp.2022.104853.
32. Wang, Z.; Yin, B.; Ruan, H.; et al. Revealing suppression effects of injection location and dose of liquid nitrogen on thermal runaway in lithium iron phosphate battery packs. *Int. J. Heat. Mass. Transf.* **2024**, *219*, 124866. https://doi.org/10.1016/j.ijheatmasstransfer.2023.124866.
33. Li, H.; Peng, W.; Yang, X.; et al. Full-Scale Experimental Study on the Combustion Behavior of Lithium Ion Battery Pack Used for Electric Vehicle. *Fire Technol.* **2020**, *56*, 2545–2564. https://doi.org/10.1007/s10694-020-00988-w.
34. Liu, T.; Hu, J.; Tao, C.; et al. Effect of parallel connection on 18650-type lithium ion battery thermal runaway propagation and active cooling prevention with water mist. *Appl. Therm. Eng.* **2021**, *184*, 116291. https://doi.org/10.1016/j.applthermaleng.2020.116291.
35. Liu, T.; Tao, C.; Wang, X. Cooling control effect of water mist on thermal runaway propagation in lithium ion battery modules. *Appl. Energy* **2020**, *267*, 115087. https://doi.org/10.1016/j.apenergy.2020.115087.
36. Ma, Y.; Zhang, Y.; Chen, N.; et al. Thermal runaway propagation behavior and cooling effect of water mist within a 18650-type LiFePO4 battery module under different conditions. *Process Saf. Environ. Prot.* **2024**, *185*, 1362–1372. https://doi.org/10.1016/j.psep.2024.04.002.
37. Zhang, L.; Duan, Q.; Xu, J.; et al. Experimental investigation on suppression of thermal runaway propagation of lithium-ion battery by intermittent spray. *J. Energy Storage* **2023**, *58*, 106434. https://doi.org/10.1016/j.est.2022.106434.

38. Andersson, P.; Arvidson, M.; Evegren, F.; et al. *Lion Fire: Extinguishment and Mitigation of Fires in Li-Ion Batteries at Sea*; RISE Report, 2018:77; RISE Research Institutes of Sweden: Gothenburg, Sweden, 2018.
39. Cui, Y.; Liu, J.; Han, X.; et al. Full-scale experimental study on suppressing lithium-ion battery pack fires from electric vehicles. *Fire Saf. J.* **2022**, *129*, 103562. https://doi.org/10.1016/j.firesaf.2022.103562.
40. Li, X.; Li, X.; Li, C.; et al. Study on the fire extinguishing effect of compressed nitrogen foam on 280 Ah lithium iron phosphate battery. *Heliyon* **2024**, *10*, e31920. https://doi.org/10.1016/j.heliyon.2024.e31920.
41. Zhang, L.; Jin, K.; Sun, J.; et al. A Review of Fire-Extinguishing Agents and Fire Suppression Strategies for Lithium-Ion Batteries Fire. *Fire Technol.* **2022**, *60*, 817–858. https://doi.org/10.1007/s10694-022-01278-3.
42. Zhao, J.; Xue, F.; Fu, Y.; et al. A comparative study on the thermal runaway inhibition of 18650 lithium-ion batteries by different fire extinguishing agents. *iScience* **2021**, *24*, 102854. https://doi.org/10.1016/j.isci.2021.102854.
43. Wang, Z.; He, C.; Geng, Z.; et al. Experimental study of thermal runaway propagation suppression of lithium-ion battery module in electric vehicle power packs. *Process Saf. Environ. Prot.* **2024**, *182*, 692–702. https://doi.org/10.1016/j.psep.2023.12.017.
44. Wang, K.; Fang, J.; Shah, H.R.; et al. Research on the influence of foaming gas in compressed air/nitrogen foam on extinguishing the n-heptane tank fire. *J. Loss Prev. Process Ind.* **2021**, *72*, 104533. https://doi.org/10.1016/j.jlp.2021.104533.
45. Wang, K.; Fang, J.; Shah, H.R.; et al. A theoretical and experimental study of extinguishing compressed air foam on an n-heptane storage tank fire with variable fuel thickness. *Process Saf. Environ. Prot.* **2020**, *138*, 117–129. https://doi.org/10.1016/j.psep.2020.03.011.
46. Guo, Y.; Chen, T.; Zhou, B.; et al. Research on Fire Suppression Characteristics of Compressed Air Foams in Full-Scale 220 kV Converter Transformer. *Fire* **2024**, *8*, 12. https://doi.org/10.3390/fire8010012.
47. Zhou, B.; Yang, W.; Yoshioka, H.; et al. Research on suppression effectiveness of compressed air foam for oil-immersed transformer hot oil fire. *Case Stud. Therm. Eng.* **2023**, *49*, 103272. https://doi.org/10.1016/j.csite.2023.103272.
48. Chen, T.; Zhang, J.; Jing, L.; et al. The experimental study of compressed air foam produced by 2-bromo-3,3,3-trifluoro-propene and air in suppression of 1 m^2 n-pentane oil fire. *Case Stud. Therm. Eng.* **2025**, *68*, 105900. https://doi.org/10.1016/j.csite.2025.105900.
49. Tian, F.; Fang, J.; Tao, S.; et al. Flame spreading and burning of high- and low-flash point fuels under compressed air foam suppression. *Case Stud. Therm. Eng.* **2024**, *64*, 105527. https://doi.org/10.1016/j.csite.2024.105527.
50. Feng, X.; Sun, J.; Ouyang, M.; et al. Characterization of penetration induced thermal runaway propagation process within a large format lithium ion battery module. *J. Power Sources* **2015**, *275*, 261–273. https://doi.org/10.1016/j.jpowsour.2014.11.017.
51. Gao, S.; Feng, X.; Lu, L.; et al. An experimental and analytical study of thermal runaway propagation in a large format lithium ion battery module with NCM pouch-cells in parallel. *Int. J. Heat Mass Transf.* **2019**, *135*, 93–103. https://doi.org/10.1016/j.ijheatmasstransfer.2019.01.125.
52. Huang, Z.; Zhao, C.; Li, H.; et al. Experimental study on thermal runaway and its propagation in the large format lithium ion battery module with two electrical connection modes. *Energy* **2020**, *205*, 117906. https://doi.org/10.1016/j.energy.2020.117906.
53. Lamb, J.; Orendorff, C.J.; Steele, L.A.M.; et al. Failure propagation in multi-cell lithium ion batteries. *J. Power Sources* **2015**, *283*, 517–523. https://doi.org/10.1016/j.jpowsour.2014.10.081.
54. Lopez, C.F.; Jeevarajan, J.A.; Mukherjee, P.P. Experimental Analysis of Thermal Runaway and Propagation in Lithium-Ion Battery Modules. *J. Electrochem. Soc.* **2015**, *162*, A1905–A1915. https://doi.org/10.1149/2.0921509jes.
55. Meng, X.; Li, S.; Fu, W.; et al. Experimental study of intermittent spray cooling on suppression for lithium iron phosphate battery fires. *eTransportation* **2022**, *11*, 100142. https://doi.org/10.1016/j.etran.2021.100142.
56. Zhang, L.; Duan, Q.; Meng, X.; et al. Experimental investigation on intermittent spray cooling and toxic hazards of lithium-ion battery thermal runaway. *Energy Convers. Manag.* **2022**, *252*, 115091. https://doi.org/10.1016/j.enconman.2021.115091.
57. *Standard No. CCCF/XFJJ-01 (2018)*; Technical Specifications for Fire Prevent and Control Equipment for Lithium Ion Battery Cabin of Electric Bus. China Certification Center for Fire Products of MEM Editor, 2018. (In Chinese)
58. Zhang, Y.; Zhao, H.; Wang, G.; et al. Effect of flame heating on thermal runaway propagation of lithium-ion batteries in confined space. *J. Energy Storage* **2024**, *78*, 110052. https://doi.org/10.1016/j.est.2023.110052.